Proceedings of the 2023 International Conference on Mathematical Physics and Computational Simulation
DOI: 10.54254/2753-8818/10/20230357

# Exploring the galactic center through gravitational microlensing: Prospects and possibilities with next-generation infrared telescopes

**Zijian (Max) Qiu[1,3,4], Peng Jiang[2,5]**

[1]Toronto Montessori School, Ontario, Canada
[2]Polar Research Institute of China, Shanghai, China
[3]Corresponding author

[4]max.yesod@gmail.com
[5]jiangpeng@pric.org.cn

**Abstract.** We aim to present a solution to the lack of observational support to our theoretical model of the Supermassive Black Hole (SMBH) and the Galactic Center (GC). To do so, we revisit the abundance of microlensing events produced by the SMBH at the GC as a fixed lens, based on the methods given by Alexander & Loeb 2001 (AL01). By applying updated observational constraints for the distribution of stars within a few arcseconds of the SMBH, we estimate the number of lensing events of distant background sources by the SMBH alone or by it and secondary stellar lenses that lie within the GC. We find our new results to be generally consistent with AL01. We predict that in any snapshot of the central ~1" region taken with a modern detection threshold of 27-28 mag, ~10 microlensed background sources will be amplified for more than 500% in brightness. As more potential microlensing events in the GC are being identified by K-band surveys with a much higher precision than previous speckled observations, we would be able to test our predictions and offer validations on the theoretical models of GC and the SMBH.

**Keywords:** microlensing, black hole, model, galactic center, Sag. A*.

## 1. Introduction

Sagittarius A*, the supermassive Black Hole (SMBH) at the galactic center (GC), has been the focus of many recent researches [1, 2], from which yielded an accurate measurement of its mass ($M_{SMBH}$=3.964±0.026×10$^6 M_{\odot}$) [3, 4] and distance ($D_0$=7946±32pc) [5, 6]. In particular, Andrea Ghez and Reinhard Genzel have been awarded the 2020 Nobel prize for their contributions on the confirmation of this SMBH [7-9]. All alone, there were estimations of galactic center stellar distribution as well as its K-band luminosity [10]. Previous attempts have been made to model the microlensing event rate in the galactic center. Nonetheless, most of them regard the optical wavelengths, and few in the IR wavelength were not able to confirm gravitational microlensing events close to the SMBH [11].

In previous works inspecting infrared sources from the region near the SMBH, it is shown that images of a distant background star initially lensed by the SMBH could be again amplified by secondary stellar lenses close to the SMBH, and produce more detectable lensing events [12]. Said secondary lensing

DOI: 10.54254/2753-8818/10/20230357

event is analogous to that applied to exploring exo planetary systems, for which during gravitational microlensing events by a stellar mass lens, the presence of surrounding planets can significantly influence the magnification of the projected image as secondary lenses [16]. In the case of Sagittarius A*, the effect of the secondary lensing would be correlated with the distance from the secondary lens to the Einstein radius of the SMBH (where the primary image should appear).

In subsequent research, more non-periodic stellar sources have been discovered through infrared observations [19-21] as well as more detailed astronomical observations of the GC [22], as candidate microlensing events. Specifically in Gallego-Cano's 2019 paper, a new updated model suggesting the Nuker model of galactic centre allows us to analyze more results from those more accurate recent surveys, we could more accurately examine the gravitational microlensing event rate around the SMBH, and thus constrain a model of the GC and the SMBH.

Since the initial prediction of the abundance of such events by Alexander & Loeb (Later on referred to as AL01), sensitivity of the new-generation instruments has been greatly increased and the model of galactic center stellar distribution has been renovated considerably [23]. For instance, the 20-hour Ultra Deep Field observation carried out in October, 2022 with the JWST was reportedly capable of detecting stars of 30 magnitude [25]. In this paper, we adopt a new model of stellar number density and luminosity distribution obtained from up-to-date observation data of GC stars [10, 26]. Thus we analyse the notable contributions of stars around the SMBH to potential microlensing events by performing analysis on the gravitational microlensing event rate near Sagittarius A*. Knowing that the light curves of gravitational microlensing events can be analyzed into the mass and kinematic properties of stars, our paper purpose an innovative approach to observationally determine the characteristics of both GC and source stars.

**Table 1.** Nanoclature.

| | |
|---|---|
| $D_0$ | The distance from observer to SMBH |
| $D_S$ | The Distance from SMBH to source |
| $R_E$ | Einstein Radius |
| $(\xi_p, \eta_p)$ | Position of Secondary Lens |
| $(\xi_i, \eta_i)$ | Position of Perturbed Image |
| $\theta_E$ | Einstein Angle |
| $\epsilon$ | The mass ratio between the secondary (GC Star) and primary lens (SMBH) |
| $x_{BH}$ | The distance from SMBH to unpurturbed image |
| A | Magnification Threshold |
| $\Sigma_*$ | Stellar Number Density at $x_{BH}$ |
| $\sigma_*$ | Cross Section Area on the Lens Plane |
| $\tau_*$ | Optical depth on the lens plane |
| $\rho_*$ | 3D Number Density on the lens plane |
| $\sigma_s$ | Cross Section Area on the Source Plane |
| $\Sigma_s$ | Stellar Number Density on the Source Plane |
| $K_0$ | Detection Limit of a Telescope |
| $K_c$ | Magnitude Cutoff |

## 2. Gravitational microlensing of distant sources by SMBH perturbed by GC stars

In our model, we consider microlensing of stellar sources in the distant background behind the SMBH. During those events, we contemplate effects of secondary lensing due to the large Einstein angle, and stellar masses which might happen to be close to the primary image to have a non-negligible magnification effect. Therefore, we focus on the case when the GC stars in front of the SMBH serve as secondary lenses, further magnifying a source image produced by SMBH primary lensing. Fig. 1 in

DOI: 10.54254/2753-8818/10/20230357

A&L shows a generalization of the setup: a second lensing event from a lens plane GC star that sources the lensed images of a background source by the SMBH. For these distant background sources, the distance from observer to SMBH ($D_0$) and that of SMBH to source ($D_S$) are comparable to each other. Thus, the Einstein radius ($R_E$) should be given by the exact form of:

$$R_E = \left(1 - \frac{D_0}{D_s}\right)^{1/2} R_\infty \tag{1}$$

or in angular measurements:

$$\theta_E = \left(1 - \frac{D_0}{D_s}\right)^{1/2} \theta_\infty \tag{2}$$

where

$$\theta_\infty = 2."02\left(\frac{M_{SMBH}}{4\times10^6 M_\odot}\right)^{1/2};\ R_\infty = D_0\theta_\infty \tag{3}$$

is the Einstein angle assuming the source is at infinite distance. Note that 1”=0.039 pc in the galactic center.

In order to evaluate the magnitude of secondary perturbation lensed by GC stars, we apply the model given by Gould & Loeb (1992): Signals from distant source is initially magnified by the SMBH, forming two unperturbed image at (angular) distance of $x_{BH}\theta_E$ to the BH on the lens plane perpendicular to the line of sight, here $x_{BH}$ is a normalized angular distance.

We suppose that the two unperturbed images are separate entities and subject to excess magnification independently, which we justify via our large Einstein angle (~1”). For the calculation regarding each of the primary images, we set it as the origin of a 2D Cartesian coordinate system with $x_{BH}$ as direction of the $x$ axis. We then have the secondary lens’ (GC star’s) location at ($\xi_p$, $\eta_p$) and the perturbed image it projects at ($\xi_i$, $\eta_i$). The unit system we implement is: The unperturbed image distance $x_{BH}$ is expressed in units of $\theta_E$, while $\xi$ and $\eta$ are expressed in units of $\sqrt{\epsilon}\theta_e$ where $\epsilon(m) = m^*/M \cdot$ is the mass ratio between the secondary (GC Star) and primary lens (SMBH). The surface area on the lens and source plane calculated are expressed respectively in units of $\epsilon\theta_E^2$ and $\theta_E^2$, while the stellar densities are also normalized to units of $[\epsilon\theta_E^2]^{-1}$ and $[\theta_E^2]^{-1}$ so that it would yield a dimensionless optical depth when finding their product.

DOI: 10.54254/2753-8818/10/20230357

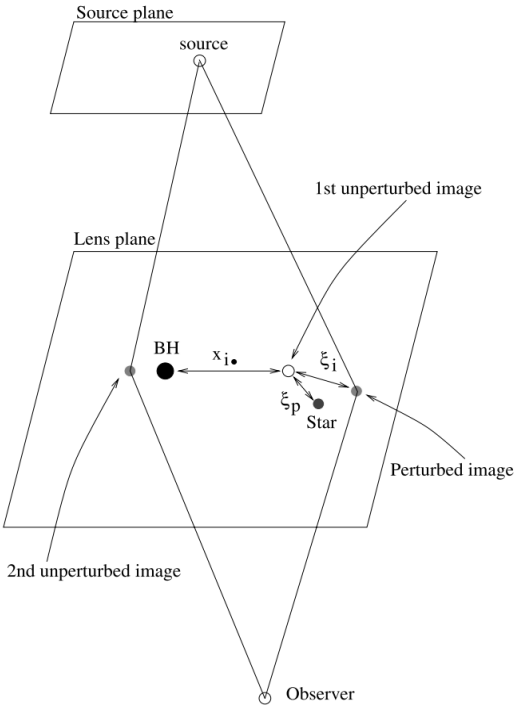


**Figure 1.** Sketch defining the notation used in this paper. The presence of a perturbing star at position $\xi_p$ relative to the unperturbed image at $x_{BH}$ splits this image into two or four images at positions $\xi_i$ relative to the unperturbed image. For clarity, only one of the multiple images, due the star, is show $\xi_i$ and the proportions are exaggerated.

The position ($\xi_i$, $\eta_i$) are given by the 2 or 4 real solutions of a quartic equation:

$$\xi_i^4 + \frac{(1-2\gamma)\xi_p}{\gamma}\xi_i^3 + \left[\frac{(1-\gamma)^2(\xi_p^2+\eta_p^2)}{4\gamma^2} - \frac{(1-\gamma)\xi_p^2}{\gamma} - \frac{1}{1+\gamma}\right]\xi_i^2 - \left[\frac{(1-\gamma)^2(\xi_p^2+\eta_p^2)\xi_p}{4\gamma^2} - \frac{(1-\gamma)\xi_p}{\gamma(1+\gamma)}\right]\xi_i - \frac{(1-2\gamma)^2\xi_p^2}{4\gamma^2(1+\gamma)} = 0 \tag{4}$$

where

$$\gamma = x_{BH}^{-2},\ \eta_i = \frac{(1+\gamma)\eta_p\xi_i}{2\xi_i\gamma + (1-\gamma)\xi_p} \tag{5}$$

while the excess magnification of the images is given by

$$A = \left|1 - \left[\gamma + (1+\gamma)^2\xi_i^2 - (1-\gamma)^2\eta_i^2\right]^2 - 4(1-\gamma^2)^2\xi_i^2\eta_i^2\right|^{-1} \tag{6}$$

$x_{BH}$ is represented in the form of gamma for simplicity sake of the formula. From the equation, we are able to determine the area of data points ($\xi_p$, $\eta_p$) that are able to produce a magnification above the threshold $A$ on the lens plane, $\sigma_*$ (> $A$, $x_{BH}$), and the optical depth of the secondary lens, or simply, the number of stellar lenses that just happen to be in this cross section that satisfies the magnification requirement:

$$\tau_*(>A, x_{BH}) = \sigma_*(>A, x_{BH})\sum_*(x_{BH}) \ll 1 \tag{7}$$

$\Sigma_*$ Here is the stellar number density at $x_{BH}$. We emphasize again that $\Sigma_*$ is usually measured in some absolute unit, but to multiply it with $\sigma_*$, which is measured in units of $\epsilon\theta_E^2$, $\Sigma_*$ must be in units of $[\epsilon\theta_E^2]^{-1}$, which involves multiplying the value of $\Sigma_*$ in absolute units by $\epsilon\theta_E^2$ per absolute unit. $\tau_*$ turns

DOI: 10.54254/2753-8818/10/20230357

out to be very small, so we assume there aren't any "double" enhancement events, that the primary image experiences lensing from multiple secondary lenses. Thus, in the small optical depth limit, probability of the background source being magnified by more than $A$, as a function of primary image location, should be:

$$P\left(>A, x_{BH}\right) \simeq \max\left[\tau_*\left(>A, x_{BH}\right), \Theta\left(A_{BH}-A\right)\right] \tag{8}$$

$\Theta$ here indicates a Heaviside step function, taking the value of 1 when $A_{BH} > A$ or 0 when $A_{BH} < A$, and $A_{BH}$ is the magnification only taking the BH into account:

$$A_{BH} = \left|1 - x_{BH}^{-4}\right|^{-1} \tag{9}$$

The probability function suggests that if $A_{BH} > A$, the SMBH itself would be sufficient to project an image at $x_{BH}$ above the required magnification, so $P$ =1. Excess magnification from secondary lenses makes an influence in the regions where the SMBH exerts smaller impact ($x_{BH}$ is far from 1 $R_E$, and $A_{BH} < A$).

Although we can follow Gould & Loeb (1992)'s method by obtaining $\sigma_*$ By reverse engineering the equation via the equi-magnification contour (since equations with powers less than 5 have analytical root-finding formulae), we decide to take another more convenient Monte-Carlo approach in this paper. For each $\gamma$ or $x_{BH}$, we uniformly scatter 10 million test points on the lens ($\xi_p$, $\eta_p$) plane and calculate the corresponding ($\xi_i$, $\eta_i$) and $A$ from Eq. 4, 5, 6. Then by counting the number of spots on the ($\xi_p$, $\eta_p$) plane which maps to an $A$ above the magnification constraint, we obtain the area $\sigma_*$ (> $A$, $x_{BH}$) as the total area multiplied by the fraction of points that satisfy the magnification constraint. Fig. 1 shows some examples of cross-sections of magnification above 300% generated by Monte Carlo tests. Left panel is for $\gamma$ = 1.3 (the primary image is within the Einstein angle) and the right panel is for $\gamma$ = 0.6 (primary image is outside the Einstein angle).

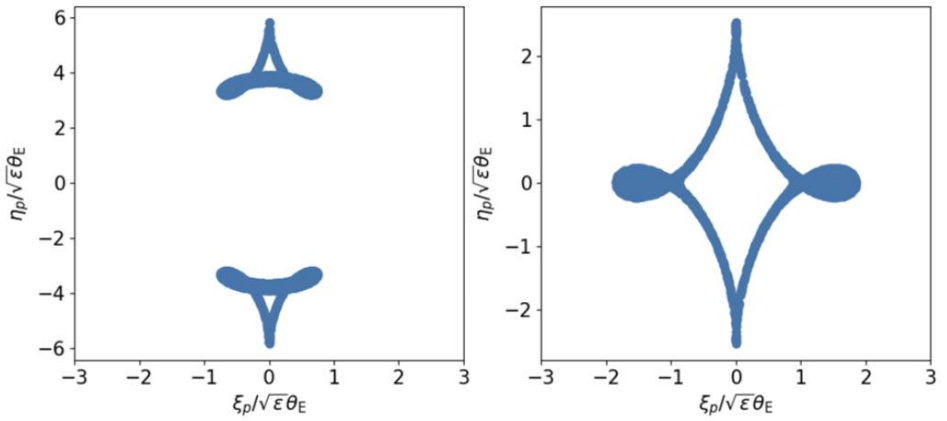


(a) (b)

**Figure 2.** Areas in the ($\xi_p$, $\eta_p$) parameter plane that satisfy the constraint of $A$ > 300% (for any of the perturbed images generated), (a): $\gamma$ = 1.3; (b): $\gamma$ = 0.6. The intrinsic shapes differ for $\gamma$ larger and smaller than 1, and approaches infinity for $\gamma$ approaching 1, these images are quite consistent with the contours from (Gould & Loeb 1992)

## 3. Surface density of secondary lenses

To obtain a stellar population model for secondary lens surface density $\sum_*(x_{BH})$, we start by assuming that all stars that could potentially act as secondary lenses, including ones undetectable in K-band wavelengths, follow a broken power law distribution as fitted by Gallego-Cano et al. (2018) from K-

DOI: 10.54254/2753-8818/10/20230357

band luminosity sources. We adopt their best-fit model parameters where $\rho_*$ is the 3D density corresponding to $\Sigma_*$(see their Table 4, ID5).

$$\rho_*(r) = \rho_*(r_b) 2^{(\beta-\Gamma)/\alpha} \left(\frac{r}{r_b}\right)^{-\Gamma} \left[1+\left(\frac{r}{r_b}\right)^{\alpha}\right]^{(\Gamma-\beta)/\alpha} \tag{10}$$

$r_b = 4.9pc$ is a break radius indicating the transition from the galactic center cusp and the galactic disk. Within $r_b$, the number density scales as $r^{-\Gamma}$, but beyond $r_b$ the number density scales as $r^{-\beta}$. In our model $\gamma$ = 1.42 and $\beta$ = 3.5, although the latter is not directly relevant to the stellar distribution close to the Einstein radius. $\alpha$ = 10 is a sharpness factor, and $\rho(r_b) = 53pc^{-3}$ is a number density of K-band luminosity sources at $r_b$.

If all stars roughly follow this distribution, we can obtain a mass density distribution of all stars, by normalizing the above profile while dictating the total mass within 1 $pc$ to be $1.1\times10^6 M_\odot$, consistent with observational values [27]. We obtain

$$\rho_*(r) = \left[1.25\times10^4 M_\odot\right] 2^{(\beta-\Gamma)/\alpha} \left(\frac{r}{r_b}\right)^{-\Gamma} \left[1+\left(\frac{r}{r_b}\right)^{\alpha}\right]^{(\Gamma-\beta)/\alpha} \tag{11}$$

This profile also suggests a total mass of $8.9\times10^6 M_\odot$within the 3.9 $pc$ region of GC; this too matches the observational values [28].

It can be shown that at $r \ll r_b$, this 3D mass density corresponds to a simplified expression for the projected 2D surface density:

$$\sum\nolimits_m(r) = \left[8.2\times10^5 M_\odot pc^{-2}\right](r/1pc)^{-0.42} \tag{12}$$

Although the stellar mass function (A. K. A, the probability distribution over stellar masses $g(m)$, with $\int g(m)dm = 1$) may be unknown, we can obtain the number density from the mass density simply by dividing an average mass $\sum_*(x_{BH}) = \sum_m(x_{BH})/\bar{m}$. We can further prove that in terms of the calculation of $\tau_*(>A, x_{BH}) = \sigma_*(>A, x_{BH})\sum_*(x_{BH})$, the average mass is indeed all we need to (e.g. solar mass $\bar{m} = M_\odot$ as usually applied in the GC) and obtain a correct result independent of $g(m)$.

This is because for an arbitrary $g(m)$, the optical depth for secondary lenses at a certain distance to the primary image ($x_{BH}$) , is the sum of the surface density from each mass bin $\sum_*(x_{BH})\, g(m)dm$ normalized from unit $[pc^{-2}]$ to unit $[\epsilon\theta_E^2]^{-1}$, multiplied by its corresponding cross section area $\sigma_*(>A, x_{BH})$ in unit of $[\epsilon\theta_E^2]$ which is independent of $g(m)$. The cross section is inherently normalized, thus always having the same value:

$$\begin{aligned}\tau_*(x_{BH}) &= \int \sum\nolimits_*(x_{BH})\, g(m)\left(\frac{m}{M_*}\theta_E^2\right)\sigma_*(x_{BH})\,dm = \sum\nolimits_*(x_{BH})\left(\theta_E^2\right)\sigma_*(x_{BH})\int g(m)\frac{m}{M_*}dm \\ &= \sum\nolimits_*(x_{BH})\left(\theta_E^2\right)\sigma_*(x_{BH})\frac{\bar{m}}{M_*} = \sum\nolimits_*(x_{BH})\left(\tilde{\text{o}}\theta_E^2\right)\sigma_*(x_{BH})\end{aligned} \tag{13}$$

Through this calculation, we show that we could propagate the cross section simply knowing the average stellar mass. Thus, we obtain the optical depth by applying an average ratio between the mean mass of star ($\bar{m} = M_\odot$)and that of the SMBH, $\epsilon$ = $2.5\times10^{-7}$, in order to rescale the unit of $\sum_*(x_{BH}) = \sum_m(x_{BH})/\bar{m}$. By doing so, the optical depth around $x_{BH}$ could be described as

$$\tau_*(x_{BH}) \equiv \frac{\sum_m(x_{BH})\left(\theta_E^2\right)\sigma_*(x_{BH})}{M_*} = \hat{\Sigma}_* x_{BH}^{-0.42}\sigma_*(x_{BH}) \tag{14}$$

via only the mass density, which is considered in section 3 as solely contributed by stars with $\bar{m}\sim m_\odot$ following the power law introduced. And $\hat{\Sigma}_*$ = 0.044 is the stellar 2D surface density at the Einstein

DOI: 10.54254/2753-8818/10/20230357

angle, normalized from unit $[pc^{-2}]$ to unit $[\epsilon\theta_E^2]^{-1}$,assuming a source distance of $D_S = 2D_0$. The power law of -0.42 indicates that $\Sigma_*$ still has a weak dependence on the distance consistent with Eqn 12.

In fact, we will show that secondary lenses located in close proximity to the SMBH Einstein radius will exert the most influence on the lensing events (Figure.3). Hence, in our region of interest $\Sigma_* \approx \hat{\Sigma}_*$ and, the influence of coefficient in the power law is relatively low.

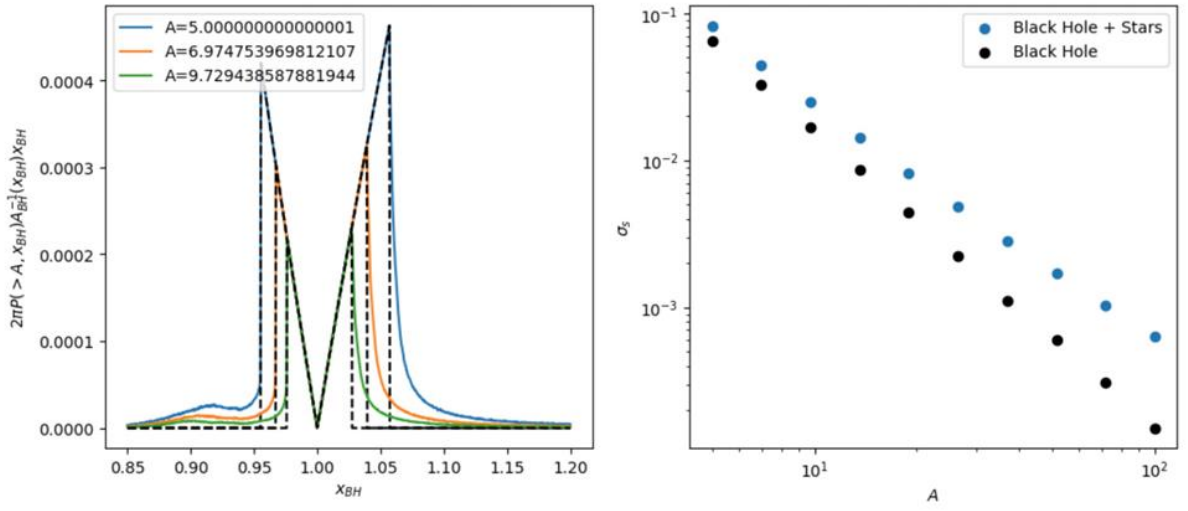


(a) (b)

**Figure 3.** Secondary lenses located in close proximity to the SMBH Einstein radius will exert the most influence on the lensing events. (a): The source plane cross section area for a source magnified by more than threshold $A$ contributed by a differential annulus in the lens plane, as a function of angular separation between primary image and SMBH $x_{BH}$. The case for SMBH+stars (bold lines) is compared to the contribution from the SMBH alone (dashed lines) for three threshold values of A; (b): total cross section $\sigma_s(>A)$ as a function of $A$, for SMBH (black dots) and SMBH+stars (blue line), integrated from $x_{BH}$ = 0.85 to $x_{BH}$ = 1.20. Both are for $\theta_E = \theta_\infty/\sqrt{2}$, assuming a source distance of $D_S = 2D_0$.

## 4. Results: optical depth of events on the source plane

By assuming the fore-mentioned stellar distribution around the SMBH and projecting the contribution per angular area onto the source plane, we could then calculate the source plane cross sectional area:

$$\sigma_s(>A) = 2\pi \int P(>A, x_{BH}) A_{BH}^{-1}(x_{BH}) x_{BH} dx_{BH} \tag{15}$$

while the function $P(>A, x_{BH})$ was given in section 2, optical depth of secondary lenses are given in section 3.

In the left panel of Fig 2 we plot the differential cross section on the source plane contributed by each annulus with a radius of $x_{BH}$ centered on the primary image location, for some characteristic magnification thresholds. Integrating this value over $x_{BH}$ will give us the total effective cross section on the source plane. The contribution by SMBH only (setting $\tau_*$ to 0) is plotted with dashed lines. As we can see, if the primary image appears very close to the Einstein radius, magnification by the SMBH is high enough for detection, thus making $P(>A)$ = 1. It is only when the primary image is further away from the Einstein radius where the secondary lens contributes to gravitational microlensing, possibly yielding images above the magnification threshold.

In the right panel of Fig 3, we plot the total cross section of the source plane over a large range of magnification threshold with blue dots. By inspection, we figured that the cross section area can be fitted with a power law of magnification such that

$$\sigma_s = 0.98A^{-1.6} \tag{16}$$

DOI: 10.54254/2753-8818/10/20230357

Comparing this with the black hole-only cross section (black dots), we see that the net contribution of stars is ~50% for $A \sim 10$, and dominates at even larger $A$.

Due to the large uncertainty in the stellar density and luminosity distribution in background stars within the Einstein radius, we implement the same power law model of generalized large-scale $K$-band luminosity distribution as that in AL01:

$$\sum\nolimits_S (< K_S) = \hat{\Sigma}_S 10^{bK_S} \tag{17}$$

where $\hat{\Sigma_s} = 5 \times 10^{-10} (\theta_E(r)/\theta_\infty)^2$ and $b = 0.4$ [29].

It can be calculated with a power-law form of cross section v.s. Magnification (Eqn 14), and an exponential form of the source luminosity function (Eqn 15), we can express the average number of lensed images that can be observed, by a telescope with detection limit of $K_0$, as

$$\begin{aligned} N_i(>A;K_0) &= \int_A^\infty dA \int_A^{K_0} dK \left|\frac{d\sigma_s}{dA}\right|_A \left|\frac{d\sum_s}{dK}\right|_{K+K_A} \\ &= \hat{\Sigma}_s \hat{\sigma}_s 10^{bK_c} A_c^{-1.6} + \frac{3.2}{5b-3.2} 10^{bK_c} \left(A_c^{2.5b-1.6} - A^{2.5b-1.6}\right) \end{aligned} \tag{18}$$

If $A \le A_c$, or else

$$= \hat{\Sigma}_s \hat{\sigma}_s 10^{bK_c} A_c^{-1.6}$$

where $K_c = 2.5 \log A_c + K_0$ is a cutoff luminosity for the source luminosity function (Eqn 15), which we take to be 28 (does not significantly affect our results).

From the Poisson distribution, we can also find out that the probability of detecting at least one event as we point the telescope towards the GC at any given time is $P = 1 - \exp(-N)$.

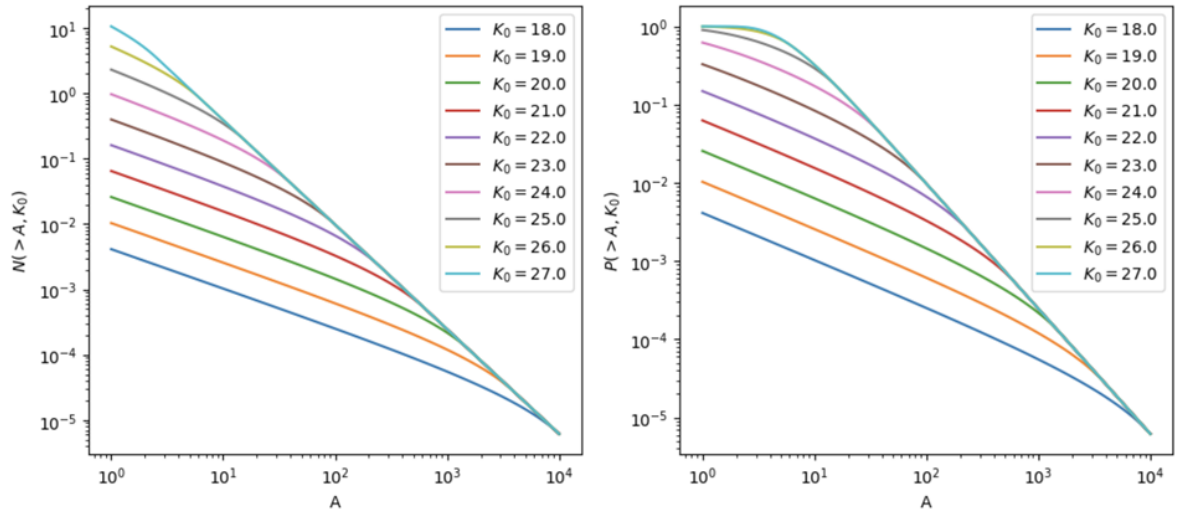


(a) (b)

**Figure 4.** The average number of lensed images and the fraction of time that at least one lensed images magnified by more than A. (a). average number of lensed images magnified by more than A that will be observed in the inner $2\theta_E$ with a limiting $K$-band magnitude $K_0$, for $D_0 = r(\theta_E = \theta_\infty/\sqrt{2})$ and $b$ = 0.4; (b): the fraction of time that at least one lensed image magnified by more than $A$, will be observed in the inner $2\theta_E$, as functions of $A$. Dotted line shows the contribution by SMBH alone, detection threshold in magnitude increasing from bottom to top.

The event number is smaller for low telescope sensitivity and high magnification requirements. At low $K_0$ (17~20), our results are similar to AL01, where $A_c$ is very large and $N$ nearly always takes the first/upper expression in Eqn 16, and both $N$ and $P$ are very small.

DOI: 10.54254/2753-8818/10/20230357

However, with current instruments like telescopes recently ready for use and prepared to launch, we can reach a detection limit of up to 27-28 magnitudes as follows [25]:

**Table 2.** Newest Generation Infrared Telescopes and Corresponding Detection Limits

| Telescope/Instrument | Detection Limit (1 Hour Obs/5 Hour Obs) |
|---|---|
| ELT/MICADO | 27.2/28.0 |
| TMT/IRIS | 27.3/28.2 |
| GMT/GMTIFS | 26.2/27.1 |
| JWST/NIRCam | 27.3/28.2 |

At such a high $K_0$ close to the cut off value of the luminosity function, only a small magnification threshold will be larger than $A_c$, and N converges to the lower expression in Eqn 16. Eventually all plotted lines of $N$ converge to this expression since it's independent of $K_0$ (because when the magnification is infinitely large one can basically detect the event with any telescope), but they converge at different $A_c$.

Additionally, the value of $N$ can become larger than 1, and $P$ will approach 1 instead of being proportional to $N$ as it is at small values. For example, when $K_0 \sim 27$, we can robustly predict that at least one image can be detected at any time in the GC, with magnification $A < 10$. But larger magnification (larger variation in lightcurve) events are harder to find, e.g. if we are looking for $A > 100$ images, the probability decreases drastically to 0.01.

## 5. Conclusion

In this paper, we study the microlensing events in the Galactic Center with SMBH acting as the primary lens, whose images are possibly additionally enhanced by the GC stars as secondary lenses. To do so, we proved that the optical depth could be calculated effectively using mean stellar mass. We apply a new and more realistic stellar surface density model that is consistent with a Nuker model fitted by observation, and obtain an enhancement effect similar to AL01 for detection thresholds of ~20mag. However, given a modern detection threshold of 27-28 magnitude, we predict that there will be a high chance that we are able to observe ~10 background sources magnified above a factor of 5 around the inner 1''(estimated Einstein's Radius) for every K-band snapshot of the region around the GC. Even if we restrict ourselves to magnifications larger than 100, we would still be able to observe a background source undergoing an event of this sort 1% of the time.

In recent years numerous microlensing campaigns towards the galactic bulge have been carried out. However, most of them are at optical wavelengths and cannot probe into the GC, but rather limited in the galactic disk. Meanwhile, modern K-Band luminosity surveys can probe into the GC central arcsec with high precision. Therefore, the prediction yielded from this paper encourages more investigation into the Einstein Radius of the SMBH to discover and record more potential microlensing events. We would be able to compare the number of events observed with our predictions and validate theoretical models of the GC and the SMBH [30][31]. If lightcurves of microlensing events detected is plotted, the mass of source objects could be deduced with the each individual lightcurve of those events. Among the detectable events, a large fraction of them will yield light-curves perturbed by stellar lenses, which will give valuable information about the mass and kinematics of these GC stars.

## References

[1] Paczynski, B. (1986). Gravitational microlensing by the Galactic Halo. The Astrophysical Journal, 304, 1.

[2] Paczyński, B. (1996). Gravitational microlensing in the Local Group. Annual Review of Astronomy and Astrophysics, 34(1), 419–459. https://doi.org/10.1146/annurev.astro.34.1.419

DOI: 10.54254/2753-8818/10/20230357

[3] Emami, R., & Loeb, A. (2020). Observational signatures of the black hole mass distribution in the Galactic Center. Journal of Cosmology and Astroparticle Physics, 2020(02), 021–021.
[4] Gillessen, S., Eisenhauer, F., Trippe, S., Alexander, T., Genzel, R., Martins, F., & Ott, T. (2009). Monitoring stellar orbits around the massive black hole in the Galactic Center. The Astrophysical Journal, 692(2), 1075–1109.
[5] Do, T., Hees, A., Ghez, A., Martinez, G. D., Chu, D. S., Jia, S., Sakai, S., Lu, J. R., Gautam, A. K., O'Neil, K. K., Becklin, E. E., Morris, M. R., Matthews, K., Nishiyama, S., Campbell, R., Chappell, S., Chen, Z., Ciurlo, A., Dehghanfar, A., … Wizinowich, P. (2019). Relativistic redshift of the star S0-2 orbiting the Galactic Center Supermassive Black Hole. Science, 365(6454), 664–668.
[6] Ghez, A. M., Klein, B. L., Morris, M., & Becklin, E. E. (1998). High proper-motion stars in the vicinity of sagittarius A*: Evidence for a supermassive black hole at the center of our galaxy. The Astrophysical Journal, 509(2), 678–686.
[7] Genzel, R., Eckart, A., Ott, T., & Eisenhauer, F. (1997). On the nature of the Dark Mass in the centre of the milky way. Monthly Notices of the Royal Astronomical Society, 291(1), 219–234.
[8] Genzel, R., Eisenhauer, F., & Gillessen, S. (2010). The Galactic Center Massive Black Hole and Nuclear Star Cluster. Reviews of Modern Physics, 82(4), 3121–3195.
[9] Ghez, A. M., Salim, S., Weinberg, N. N., Lu, J. R., Do, T., Dunn, J. K., Matthews, K., Morris, M. R., Yelda, S., Becklin, E. E., Kremenek, T., Milosavljevic, M., & Naiman, J. (2008). Measuring distance and properties of the milky way's central supermassive black hole with stellar orbits. The Astrophysical Journal, 689(2), 1044–1062.
[10] Gallego-Cano, E., Schödel, R., Dong, H., Nogueras-Lara, F., Gallego-Calvente, A. T., Amaro-Seoane, P., & Baumgardt, H. (2017). The distribution of stars around the milky way's central Black Hole. Astronomy & Astrophysics, 609.
[11] Shvartzvald, Y., Bryden, G., Gould, A., Henderson, C. B., Howell, S. B., & Beichman, C. (2017). UKIRT MICROLENSING SURVEYS AS A PATHFINDER FOR WFIRST: THE DETECTION OF FIVE HIGHLY EXTINGUISHED LOW-|b| EVENTS. The Astronomical Journal, 153(2), 61.
[12] Chaname, J., Gould, A., & Miralda-Escude, J. (2001). Microlensing by stellar black holes around sagittarius A*. The Astrophysical Journal, 563(2), 793–799.
[13] Navarro, M. G., Minniti, D., & Contreras-Ramos, R. (2018). VVV survey microlensing: The Galactic Longitude Dependence. The Astrophysical Journal, 865(1).
[14] Navarro, M. G., Minniti, D., & Ramos, R. C. (2017). VVV survey microlensing events in the Galactic Center Region. The Astrophysical Journal, 851(1).
[15] Sumi, T., Bennett, D. P., Bond, I. A., Abe, F., Botzler, C. S., Fukui, A., Furusawa, K., Itow, Y., Ling, C. H., Masuda, K., Matsubara, Y., Muraki, Y., Ohnishi, K., Rattenbury, N., Saito, T., Sullivan, D. J., Suzuki, D., Sweatman, W. L., Tristram, P. J., … Yock, P. C. (2013). The microlensing event rate and optical depth toward the galactic bulge from Moa-II. The Astrophysical Journal, 778(2), 150.
[16] Gould, A., & Loeb, A. (1992). Discovering planetary systems through gravitational microlenses. The Astrophysical Journal, 396, 104.
[17] Mao, S., & Paczynski, B. (1991). Gravitational microlensing by Double stars and planetary systems. The Astrophysical Journal, 374.
[18] Miralda-Escude, J., & Gould, A. (2000). A cluster of black holes at the Galactic Center. The Astrophysical Journal, 545(2), 847–853.
[19] Rafelski, M., Ghez, A. M., Hornstein, S. D., Lu, J. R., & Morris, M. (2007). Photometric stellar variability in the Galactic Center. The Astrophysical Journal, 659(2), 1241–1256.
[20] Schödel, R., Eckart, A., Alexander, T., Merritt, D., Genzel, R., Sternberg, A., Meyer, L., Kul, F., Moultaka, J., Ott, T., & Straubmeier, C. (2007). The structure of the nuclear stellar cluster of the milky way. Astronomy & Astrophysics, 469(1), 125–146.

DOI: 10.54254/2753-8818/10/20230357

[21] Schödel, R., Gallego-Cano, E., Dong, H., Nogueras-Lara, F., Gallego-Calvente, A. T., Amaro-Seoane, P., & Baumgardt, H. (2017). The distribution of stars around the milky way's central Black Hole. Astronomy & Astrophysics, 609.

[22] Gautam, A. K., Do, T., Ghez, A. M., Morris, M. R., Martinez, G. D., Hosek, M. W., Lu, J. R., Sakai, S., Witzel, G., Jia, S., Becklin, E. E., & Matthews, K. (2019). An adaptive optics survey of stellar variability at the Galactic Center. The Astrophysical Journal, 871(1), 103.

[23] Baumgardt, H., Amaro-Seoane, P., & Schödel, R. (2017). The distribution of stars around the milky way's central Black Hole. Astronomy & Astrophysics, 609.

[24] Lam, C. Y., Lu, J. R., Hosek, M. W., Dawson, W. A., & Golovich, N. R. (2020). PopSyCLE: A new population synthesis code for compact object microlensing events. The Astrophysical Journal, 889(1).

[25] Michałowski, M. J., & Mróz, P. (2021). Stars lensed by the supermassive black hole in the center of the milky way: Predictions for ELT, TMT, GMT, and JWST. The Astrophysical Journal Letters, 915(2).

[26] Hopman, C., & Alexander, T. (2006). The effect of mass segregation on gravitational wave sources near massive black holes. The Astrophysical Journal, 645(2).

[27] Schödel, R., Merritt, D., & Eckart, A. (2009). The nuclear star cluster of the milky way: Proper motions and mass. Astronomy & Astrophysics, 502(1), 91–111.

[28] Chatzopoulos, S., Fritz, T. K., Gerhard, O., Gillessen, S., Wegg, C., Genzel, R., & Pfuhl, O. (2014). The old nuclear star cluster in the milky way: Dynamics, mass, statistical parallax, and Black Hole Mass. Monthly Notices of the Royal Astronomical Society, 447(1), 948–968.

[29] Alexander, T., & Loeb, A. (2001). Enhanced microlensing by stars around the Black Hole in the Galactic Center. The Astrophysical Journal, 551(1), 223–230.

[30] Feldmeier, A., Neumayer, N., Seth, A., Schödel, R., Lützgendorf, N., de Zeeuw, P. T., Kissler-Patig, M., Nishiyama, S., & Walcher, C. J. (2014). Large scale kinematics and dynamical modelling of the milky way nuclear star cluster. Astronomy & Astrophysics, 570.

[31] Fritz, T. K., Chatzopoulos, S., Gerhard, O., Gillessen, S., Genzel, R., Pfuhl, O., Tacchella, S., Eisenhauer, F., & Ott, T. (2016). The nuclear cluster of the milky way: Total mass and luminosity. The Astrophysical Journal, 821(1), 44.